JOURNAL OF MAGNETIC RESONANCE **132,** 144–149 (1998)
ARTICLE NO. MN981408

Pulsed Gradient NMR Probes for Solid State Studies

Wurong Zhang and D. G. Cory[1]

Department of Nuclear Engineering, Massachusetts Institute of Technology, Cambridge, Massachusetts 02139

Received December 17, 1997

Recently introduced studies of the spatial characteristics of spin dynamics in dipolarly coupled solids rely upon NMR probes with strong magnetic field gradients to create spatial magnetization gratings with periods of from 1 μm to 1 nm. The measurements are carried out as scattering experiments where the spatial displacement of spin coherence is recorded as a phase shift or attenuation of the magnetization grating. Recently we have employed these techniques to make a direct measurement of the spin diffusion rate in single crystal CaF_2. Here we discuss designs for strong pulsed gradient NMR probes. Three gradient coil sets were designed and constructed, with coil constants of 0.32, 0.67, and 4.15 T/m/A. When driven by a pulsed current source that provides up to 300 A, pulsed gradients of 100, 200, and 600 T/m, respectively, were generated. These designs are fully described, along with practical issues of coil heating and probe stability.

1. INTRODUCTION

Magnetic field gradients are widely employed in NMR (*1*) for imaging, diffusion studies, coherent pathway selection, and solvent suppression, and recently we have shown that with sufficiently strong gradients they can be used to explore the structure and dynamics of dipolarly coupled spins via high-resolution NMR scattering experiments (*2*). An NMR scattering experiment involves the creation of a spatial magnetization grating, a period of spin evolution including the displacement of spin magnetization, and finally detection of the residual magnetization grating. When the spatial offsets are small (such as when they are driven by dipolar coupling), large gradients are required since only very fine gratings will be sensitive to the small offsets.

Large static magnetic field gradients are well known in NMR experiments with the gradients originating either from the fringe fields of large magnets or from the magnetic properties of the sample itself. Genack and Redfield (*3, 4*) studied the dipolar energy dissipation and nuclear spin diffusion under static gradients of more than 10^5 T/m by looking near the surface of a type II superconductor. Samoilenko *et al.* (*5*) used the stray field of 30 T/m near the end of a superconducting solenoid for subsurface imaging of solids. Kimmich *et al.* (*6*) used the fringe fields of 10 and 42 T/m of superconducting magnets for measuring small self-diffusion coefficients, including studies (*7*) with fringe fields of 32 and 60 T/m where spin diffusion was observed in melts of entangled polymers. Using force detection, Züger *et al.* (*8*) recorded three-dimensional images of an ammonium nitrate sample with a gradient of 2200 T/m generated by a small nearby magnetic particle, and Schaff and Veeman (*9*) have also used force detection with a gradient of 500 T/m generated with a somewhat larger magnetic particle. Although static gradients have the advantages of high strength, excellent stability, and no heating, they are difficult to combine with multiple-pulse coherent averaging, since the offset dependence of such methods complicates the creation of a spatially uniform grating. For these applications, pulsed gradients have an advantage since it is known how to combine them with multiple pulse cycles while avoiding offset variations (*10–12*). Unfortunately, pulsed gradients are generally much weaker than static gradients.

Pulsed magnetic field gradients are routinely used in spatial NMR experiments and various designs are well known, including Stejskal and Tanner's design of a pulsed Maxwell pair at 1 T/m for diffusion studies (*13, 14*), and Karlicek and Lowe's quadrupole gradient set of 16 T/m for diffusion measurements in samples with small diffusion coefficients (*15*). For microscopy studies, pulsed gradients on the order of 10 T/m are widely used (*1, 16*). For solid-state scattering experiments, however, gradients stronger than 100 T/m are necessary.

The essence of NMR scattering is to record the extent or variance of microscopic displacement of spin coherence by directly observing the amplitude and phase changes of a well-defined spin magnetization grating. In solid-state scattering experiments, this is driven by the dipole–dipole interaction. The process is slow and the characteristic length of the magnetization grating has to be on the order of the root mean square displacement during the spin–lattice relaxation time ($\sqrt{2DT_1}$). In the case of a ^{1}H- or ^{19}F-rich rigid solid, the spin diffusion coefficient, D, is of order 10^{-4} $\mu m^2/s$. The gradient pulse width is limited in solid-state NMR experiments by the size of windows in multiple pulse cycles, and, in the simplest case, the pitch

[1] To whom correspondence should be addressed. NW14-4111, 150 Albany Street, Cambridge, MA 02139. Fax: (617)253-5405. E-mail: dcory@mit.edu.

1090-7807/98 $25.00

of a grating is inversely proportional to the first moment of the gradient waveform. With a gradient of 100 T/m, a total time of ~25 ms is needed to create a magnetization grating with a pitch of 10 nm.

2. GRADIENT COIL DESIGN

Typically $\partial B_z/\partial z$ gradient coils have one of two symmetries, a Maxwell pair (*14*) or a quadrupole (*15*), and the general features have been described by Suits and Wilken (*17*). For the designs used here the Maxwell pair geometry is prefered since it is easier to construct at very small dimensions, and good gradient profiles are obtained with very few turns. A Maxwell pair consists of a set of circular loops with currents of equal amplitudes but opposite directions, and it generates magnetic field gradients symmetric about the midplane and about the central axis. For two current loops with radii of r_0, centered at $z = \pm z_0$, the gradient may be calculated via the Biot–Savart Law as

$$\frac{\partial B_z(r, z)}{\partial z} = \frac{3\mu I r_0}{4\pi}\int_0^{2\pi} d\varphi'(r_0 - r\cos\varphi') \times \left\{\frac{z_0 - z}{[r^2 + r_0^2 - 2rr_0\cos\varphi' + (z_0 - z)^2]^{5/2}} + \frac{z_0 + z}{[r^2 + r_0^2 - 2rr_0\cos\varphi' + (z_0 + z)^2]^{5/2}}\right\}, \quad [1]$$

where μ is the permeability of the sample. Equation [1] can be used to calculate the gradient profile and the gradient coil constant (T/m/A). The gradient at the center of a single-turn Maxwell pair is

$$G_1 = \frac{12\beta\mu I}{(1 + \beta^2)^{5/2}D^2}, \quad [2]$$

where D is the diameter of the coil and $\beta = 2z_0/D$. For the largest volume of useful linear gradients β is chosen to be 0.866 since this geometry eliminates the third-order as well as all even-order expansion terms in the magnetic field as a function of offset along z (*14, 17*). The average coil constant, G_1/I, is inversely proportional to D^2 for a single-turn Maxwell pair. At small dimensions, large coil constants are easily obtained; for example, with $\mu \sim 4\pi \times 10^{-7}$ N/A^2, if $D = 1$ mm, then $G_1/I \approx 3.22$ T/m/A, and 300 A will generate a gradient of ~1000 T/m.

When higher coil constants and better gradient homogeneity are desired, more turns and carefully placed multiple wirings are necessary. Suits and Wilken (*17*) analyzed the field along the central axis and found that, for a gradient coil constructed by double blocks of Maxwell pairs, with Z_1, Z_2 defined as the distance of the first and second block from the center, respectively, R defined as the radius of the current loop, and S_2/S_1 defined as the current ratio between the second and the first block, for the conditions $Z_1 = 0.44\ R$, $Z_2 = 1.19\ R$, $S_2/S_1 = 7.47$, the third-order, fifth-order, seventh-order, and all even-order expansion terms in the magnetic field are eliminated.

3. THE TEMPERATURE INCREASE

The large pulsed currents required for strong gradients lead to coil heating which, in addition to raising the temperature of the gradient coil, changes its resistance and leads to current decreases when used with a voltage source. The heat dissipation may also raise the temperature and resistance of the nearby RF coil, thereby detuning the resonance circuit. In the following we will employ a simple calculation of coil heating that assumes there is no heat transfer to the coil form and thus represents a worst-case analysis.

In our experiments a voltage source V has been used since it is stable, readily available, and inexpensive. The gradient coil is constructed from copper wire with a mass of m_g and a resistance of R_g. Some of the properties of copper at room temperature are density $\rho \approx 6.4 \times 10^4$ kg/m^3, heat capacity $q_c \approx 4.2 \times 10^2$ J/kg·°C, resistivity $\rho_r \approx 1.724 \times 10^{-8}\ \Omega$m, and temperature coefficient of resistivity $\alpha \approx 3.93 \times 10^{-3}$/°C. If both the on-resistance due to all parts of the circuit other than the gradient coil, R_o, and the coil resistance, R_g, increase by the same factor, then the temperature changes follow the differential equation

$$\left\{\frac{V}{(R_o + R_g)[1 + \alpha(T - T_0)]}\right\}^2 \times R_g[1 + \alpha(T - T_0)]dt = m_g q_c dT, \quad [3]$$

which has a solution for the temperature raise from ambient of

$$\Delta T = \alpha^{-1}\left\{\sqrt{1 + \frac{2\alpha V^2 R_g \Delta t}{(R_o + R_g)^2 m_g q_c}} - 1\right\}, \quad [4]$$

where Δt is the total on time.

For practical coils, $2V^2R_g\Delta t/(R_o + R_g)^2 m_g q_c \ll \alpha^{-1}$ (≈254°C), which permits the simplification to

$$\Delta T \approx \frac{V^2 R_g \Delta t}{(R_o + R_g)^2 m_g q_c}. \quad [5]$$

Equation [5] describes the temperature increase due to heat dissipation in the coil when the resistance change is not an important contribution. For an n-turn Maxwell pair ($2n$ turns in total) with an average coil diameter D, wire diameter

d, $m_g \approx n\pi^2\rho d^2 D/2$, $R_g \approx 8nD\rho_r/d^2$, and assuming that all resistance arises from the coil,

$$\Delta T \approx (4\pi^2\rho\rho_r q_c)^{-1}\frac{V^2\Delta t}{n^2D^2} \approx 0.055\frac{V^2\Delta t}{n^2D^2}, \qquad [6]$$

where SI units are used for all variables. To a good approximation, the temperature increase is independent of the wire diameter, but is inversely proportional to n^2 and D^2.

4. THE RATIO OF THE GRATING WAVENUMBER TO THE COIL TEMPERATURE INCREASE

In solid-state scattering experiments, large-wavenumber gratings are required; however, the coil temperature increases must be limited. It is useful therefore to consider the ratio of the grating wavenumber k ($k = \gamma G\Delta t$, where γ is the gyromagnetic ratio, G is the gradient strength, and Δt is the gradient pulse length) to the coil temperature increase ΔT as a measure of the coil performance. For the n-turn Maxwell pair geometry, a general result may be derived for this ratio in the case where the gradient scales as the square root of the number of turns,

$$\frac{k}{\Delta T} \approx 6\pi^2\rho q_c\mu\frac{\gamma\beta n^{3/2}d^2}{(1+\beta^2)^{5/2}VD} \approx \frac{2000\gamma\beta n^{3/2}d^2}{(1+\beta^2)^{5/2}VD}, \qquad [7]$$

where again SI units are used for all variables. The optimal geometry is then small coils, low source voltages, and large wire diameters with multiple turns. Clearly, there is the additional requirement that a sufficient volume must be provided to contain a detectable number of spins.

5. LORENTZ FORCES AND ASSOCIATED TORQUES

Regardless of the details of the coil design, pulsed currents of more than 100 A are delivered in a static magnetic field of ~10 T, resulting in strong Lorentz forces and their associated torques. There is no net force or torque on a current loop that is symmetrically arranged in a magnetic field; however, the current paths that connect to these loops cannot all be parallel to the external field and the forces on these must be sustained.

In our design, illustrated in Fig. 1, the input and return current paths are each about 2.5 cm long and are perpendicular to an external field of ~6 T. With a current of 300 A, the Lorentz force is ~45 N. Since the two paths are about 30° apart, the net force is ~23 N, and with a distance between the two paths of ~8 mm the total torque is ~0.35 N·m. As an example, consider a single-turn gradient coil constructed from a brass rod, shown in Fig. 2, with an inner diameter of $d_i = 1.4$ mm, an outer diameter of $d_o = 5.0$ mm, and a length of $l = 8.8$ mm. Ignoring any asymmetry in this design, the moment of inertia with respect to the center of the cylinder is

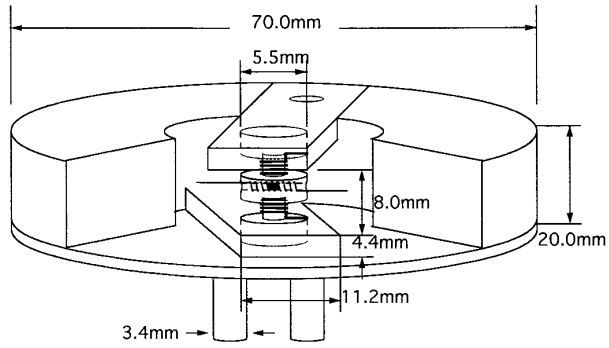

FIG. 1. A schematic diagram of the gradient set holder. The frame was machined from G-10 and solidly fixed to the probe body. Two copper blocks are fitted into the G-10 frame to support the gradient coil. Current through the probe is provided by the two copper rods fixed to the copper block. The gradient coil is glued to the frame and its leads are soldered to the copper blocks.

$J = \int_{-l/2}^{l/2} z^2\rho(\pi/4)(d_o^2 - d_i^2)dz = \pi\rho(d_o^2 - d_i^2)l^3/48 \approx 6\times10^{-8}$ kg·m^2. With a torque of $T = 0.35$ N·m acting on its body, the initial angular acceleration would be $\ddot{\theta} = T/J \approx 7\times10^6$ rad/s^2 (~1 cycle/ms^2) if there were no support!

Any motion of the sample relative to the gradient coil introduces errors in refocusing the spin magnetization grating. A sample size of 500 μm with a grating of 1 nm requires a precision of ~1 in 10^6. Fortunately, in solid samples any motions are of the entire sample relative to the gradient set and hence only a phase shift is introduced. So while the sample need not be held to within the pitch of the grating, a robust gradient holder is still necessary. For this work it was constructed out of a fiberglass composite and is illustrated in Fig. 1.

6. THREE GRADIENT SETS

For an optimal coil the gradient strength, temperature increase, $k/\Delta T$, Lorentz forces, and torques must be considered together. In general, larger numbers of turns improve the performance for all of these factors. Larger wire diameter d and larger coil diameter D increase the ratio of $k/\Delta T$, but they also reduce the gradient coil constant, so some tradeoffs have to be made.

Sprenger and Cory (*18*) have presented a preliminary design of a single-turn Maxwell pair machined directly from a copper rod, which has a coil constant of ~0.35 T/m/A and a sample diameter of ~0.5 mm. In this work, a modified version of the single-turn gradient coil was designed and constructed from a brass rod and cemented to a fiberglass composite for rigidity. The new design maintains nearly the same coil constant (~0.32 T/m/A), but allows larger sample volume (0.80 mm in diameter) and has a gradient homogeneity of approximately ±5% in the sample region. The details of the new design are illustrated in Fig. 2. Generally, this design has the advantages of being easily machined,

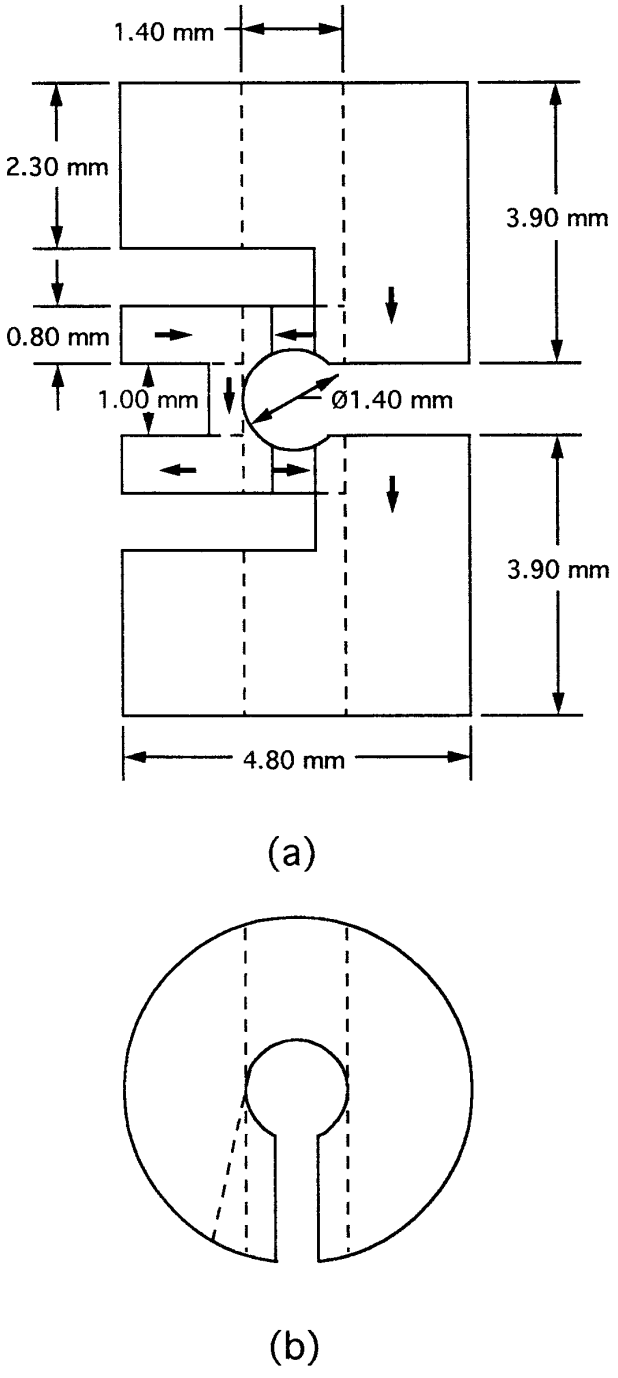

FIG. 2. A single-turn gradient coil set machined from a cylindrical brass rod. The calibrated average coil constant is ~0.32 T/m/A. AWG34 wires with a diameter of ~0.18 mm can be used for the RF coil. The sample tube has an outer diameter of 1.00 mm and an inner diameter of 0.80 mm. (a) Side view of the gradient coil. The arrows show the current directions. The head and the bottom are soldering to the copper blocks shown in Fig. 1. The central part is a single-turn Maxwell pair. (b) Top view of the central Maxwell pair.

having a large effective wire diameter and very small resistance, requiring a low source voltage, and not suffering much from coil heating. The disadvantages are a low coil constant, relatively poor homogeneity, and the large currents required, which introduce large Lorentz forces and torques.

For the measurement of the spin diffusion coefficient in single-crystal CaF_2, a four-turn Maxwell pair gradient coil set was used. The current loops were wound on a coil frame, as shown in Fig. 3. The calculated gradient profile in the sample region is well confined to 0.68 T/m/A ± 2.0%. The average coil constant was calibrated by self-diffusion measurements in water to be (0.67 ± 0.02) T/m/A. This gradient set has both a higher coil constant and a greater homogeneity. The prices paid are a smaller wire diameter and larger resistance, and therefore more heat dissipation. Nevertheless, the upper limit of the temperature increase of the gradient coil in the spin diffusion measurement at $k \approx 10\ \mu m^{-1}$ was less than 2°C.

Even larger coil constants and better gradient linearity were realized by a third gradient set constructed from two building blocks to approximate the ideal conditions described by Suits and Wilken (*17*). Figure 4 shows the configuration where 31 turns were wound on each side of the coil frame. The calculated coil constant is 4.01 T/m/A with a homogeneity of ±0.6%. The average coil constant was calibrated again by self-diffusion measurements in water and found to be (4.15 ± 0.04) T/m/A. Lower currents are required in this design and thus smaller Lorentz forces and associated torques. Heat dissipation is naturally higher. These three gradient sets are compared in Table 1.

One of the important experimental issues for scattering experiments is the temperature rise of the gradient coil since this directly affects the gradient calibration. For the 31-turn

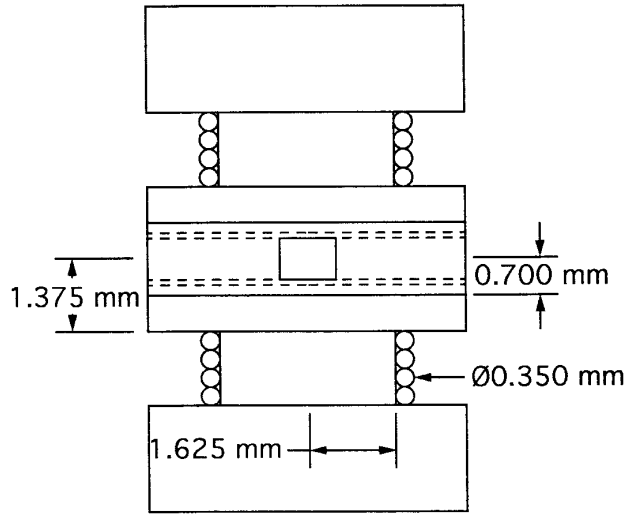

FIG. 3. A gradient coil set with four turns on each side of the Maxwell pair. The dotted lines denote the sample tube with an outer diameter of 1.00 mm and inner diameter of 0.80 mm. AWG28 wires with a diameter of ~0.35 mm were used for the gradient coil and AWG34 wires with a diameter of ~0.18 mm were used for the RF coil. The calculated coil constant for a sample region of diameter 0.80 mm and length 1.00 mm is 0.68 T/m/A ± 2%, and the calibrated average coil constant is 0.67 T/m/A.

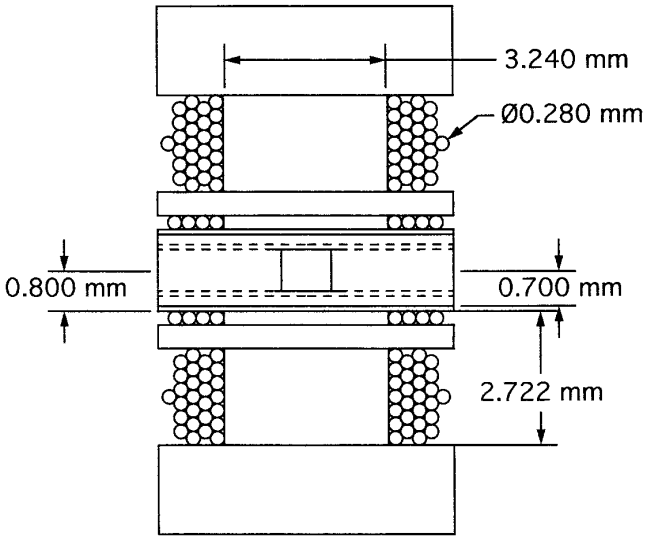

FIG. 4. A gradient coil set designed for higher coil constant and better gradient profile. The dotted lines denote the sample tube with an outer diameter of 1.00 mm and an inner diameter of 0.80 mm. AWG30 wires with a diameter of ~0.28 mm were used for the gradient coil, whereas AWG34 wires with a diameter of ~0.18 mm were used for the RF coil. The calculated coil constant for a sample region of diameter 0.80 mm and length 1.00 mm is 4.01 T/m/A ± 0.6%, and the calibrated average coil constant is 4.15 T/m/A.

gradient set, with 30-gauge wire, a total wire length of 0.90 m, $m_g \approx 2.92 \times 10^{-3}$ kg and $R_g \approx 0.31\ \Omega$, and a voltage source of 48 V (corresponding to ~140 A), a total current on time of ~12 ms is necessary and an upper limit of the temperature increase of ~60°C is expected for the creation of a magnetization grating with a period of 3 nm.

In an experiment where 64 current pulses of 200 μs each and a spacing of 400 μs were applied, the measured temperature increase was ~40°C and observed gradient coil current dropped from ~140 A to ~100 A. About half of this current drop was due not to the coil resistance change, but to the insufficient recovery of the capacitors in the current-providing circuit described in the next section.

7. A CIRCUIT FOR PROVIDING LARGE PULSED CURRENTS

Conradi *et al.* (*19*) introduced a circuit to generate short, intense gradient pulses for solid-state imaging. The gradient pulses were as short as a few microseconds, and voltage sources of ~100 V were used to generate pulsed currents of ~20 A. In our design, the requirement for the gradient pulse length is looser and so lower voltage sources can be used to generate much larger currents. Figure 5 shows the circuit for generating large pulsed currents, using car batteries as the voltage source, and four large storage capacitors (each 4800 μF) in parallel to suppress spikes during switching. The bridge circuit is switched by a set of power MOSFETs. FETs 1A and 1B provide pulsed currents in one direction, and FETs 2A and 2B do so in the opposite direction. FET 3 and a variable resistor R1 provide small pulsed currents for accurate adjustment purposes. The power MOSFETs are Harris Semiconductor RFA100N05E, each of which has an on-resistance of 8 mΩ and an allowed maximum pulsed current of 300 A. To protect against current overdrive, three FETs are used in parallel. Since the switching time of each FET is much faster than the current rise time of the circuit (limited by the large capacitance), the three parallel FETs can be turned on nearly simultaneously, and the on-resonances of the switches are correspondingly decreased by a factor of 3. A 10-mΩ shunt R2 is included in the circuit for accurate calibration of the current amplitudes, and all other connections, other than the gradient coil, contributed less than 10 mΩ resistance.

TABLE 1
Compiled Features of Three Gradient Sets

Gradient coil set	Single-turn	4-turn	31-turn
Wire resistance	<3 mΩ (brass)	20 mΩ	310 mΩ
Sample diameter	0.8 mm	0.8 mm	0.8 mm
Sample length	1.0 mm	1.0 mm	1.0 mm
Coil constant	0.32 T/m/A	0.67 T/m/A	4.15 T/m/A
Gradient homogeneity	±5%	±2%	±0.6%
Current	300 A	300 A	140 A
Lorentz force	Large	Large	Smaller
Gradient strength	~100 T/m	~200 T/m	~600 T/m

With a 12-V car battery, pulsed currents of ~300 A were delivered to the single-turn gradient coil, and currents of more than 200 A were delivered to the four-turn gradient coil. With two 12-V car batteries in series, currents of ~300 A were delivered to the four-turn gradient coil; with four 12-V car batteries, currents of ~140 A were delivered to the 31-turn gradient coil. The maximum gradient strengths achieved with these three gradient sets are 100, 200, and 600 T/m.

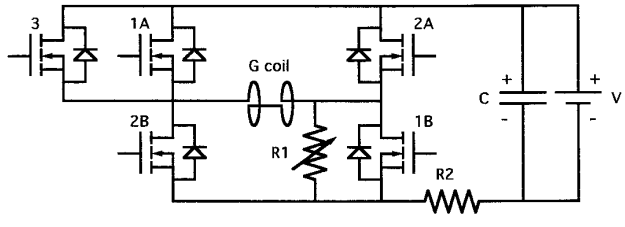

FIG. 5. The bridge circuit for switching large currents. A voltage source V is used to supply pulsed currents, and large storage capacitors are used to suppress spikes during switching. The bridge circuit is switched by a set of power MOSFETs. FETs 1A and 1B provide pulsed currents in one direction, while FETs 2A and 2B do so in the opposite direction. FET 3 and a variable resistor R1 provide small pulsed currents for accurate adjustment purposes. A 10-mΩ shunt R2 is included in the circuit for accurate calibration of the current amplitudes.

These gradients can create spatial magnetization gratings with periods as fine as 1 nm, for the first time permitting magnetization transport to be followed over length scales appropriate to the dipolar interaction. The first use was to perform a direct measurement of the small spin diffusion coefficients (on the order of 10^{-4} $\mu m^2/s$) in single-crystal CaF_2 by carefully measuring the attenuation rate of a well-created magnetization grating (*2*) with a dipolar decoupled pulsed gradient spin echo sequence. These gradient developments will allow us to implement high-resolution NMR scattering experiments aimed at the accurate measurement of the local distribution of internuclear distances between selected spins over length scales of 5 to 250 Å, as well as the study of spin dynamics over this same spatial range.

ACKNOWLEDGMENTS

The research was supported in part by the National Science Foundation (DMR-9357603), the Center for Materials Science and Engineering at MIT, and the National Institutes of Health (RR-00995).

REFERENCES

1. P. T. Callaghan, ''Principles of Nuclear Magnetic Resonance Microscopy,'' Clarendon, Oxford (1991).
2. W. Zhang and D. G. Cory, *Phys. Rev. Lett.* **80,** 1324 (1998).
3. A. Z. Genack and A. G. Redfield, *Phys. Rev. B* **12,** 78 (1975).
4. A. G. Genack, *Phys. Rev. B* **13,** 68 (1976).
5. A. A. Samoilenko, D. Yu. Artemov, and L. A. Silbel'dina, *JETP Lett.* **47,** 417 (1988).
6. R. Kimmich, W. Unrath, G. Schnur, and E. Rommel, *J. Magn. Reson.* **91,** 136 (1991).
7. E. Fischer, R. Kimmich, and N. Fatkullin, *J. Chem. Phys.* **106,** 9883 (1997).
8. O. Züger, S. T. Hoen, C. S. Yannoni, and D. Rugar, *J. Appl. Phys.* **79,** 1881 (1996).
9. A. Schaff and W. Veeman, *J. Magn. Reson.* **126,** 200 (1997).
10. D. G. Cory, J. B. Miller, R. Turner, and A. N. Garroway, *Mol. Phys.* **70,** 331 (1990).
11. S. Matsui, *Chem. Phys. Lett.* **179,** 187 (1991).
12. M. S. Crawford, B. C. Gerstein, A.-L. Kuo, and C. G. Wade, *J. Am. Chem. Soc.* **102,** 3728 (1980).
13. E. O. Stejskal and J. E. Tanner, *J. Chem. Phys.* **42,** 288 (1965).
14. J. E. Tanner, *Rev. Sci. Instrum.* **36,** 1086 (1965).
15. R. F. Karlicek, Jr., and I. J. Lowe, *J. Magn. Reson.* **37,** 75 (1980).
16. S. Choi, X.-W. Tang, and D. G. Cory, *Int. J. Imaging Syst. Technol.* **8,** 263 (1997).
17. B. H. Suits and D. E. Wilken, *J. Phys. E: Sci. Instrum.* **22,** 565 (1989).
18. P. Sprenger and D. G. Cory, Presentation at the Experimental NMR Conference, Boston (1995).
19. M. Conradi, A. N. Garroway, D. G. Cory, and J. B. Miller, *J. Magn. Reson.* **94,** 370 (1991).